Journal of Materials Chemistry C

PAPER

View Article Online
View Journal | View Issue

Cite this: J. Mater. Chem. C, 2015, 3, 1929

Visible light detectors based on individual $ZrSe_3$ and $HfSe_3$ nanobelts

Wei-Wei Xiong, Jin-Qiang Chen, Xing-Cai Wu* and Jun-Jie Zhu*

Received 2nd November 2014
Accepted 15th December 2014

DOI: 10.1039/c4tc02492c

www.rsc.org/MaterialsC

Zinc triselenide ($ZrSe_3$) and hafnium triselenide ($HfSe_3$) nanobelts were synthesized using a chemical vapor transport method. Photodetectors based on individual nanobelts of $ZrSe_3$ and $HfSe_3$ were fabricated on SiO_2/Si substrates, respectively, and the optoelectronic properties of both were evaluated. The $ZrSe_3$ nanobelt photodetector showed a good photoresponse to wavelengths ranging from 405 nm to 780 nm. Under illumination with 650 nm light, the ratio of photoswitch currents reached 1.97 with a light on/off period of 50 s at a bias voltage of 5 V. The $HfSe_3$ nanobelt photodetector also showed good photoresponse to wavelengths ranging from 405 nm to 650 nm, and the ratio of photoswitch currents, under illumination with 532 nm light, reached 2.2 with a light on/off period of 50 s at a bias voltage of 5 V. The photoresponse time of both the photodetectors was less than 0.4 s. The results demonstrated that $ZrSe_3$ and $HfSe_3$ nanobelts possessed excellent photoconductivity, and suggested that these photodetectors would have potential applications under a range of visible light conditions.

Introduction

With developments in microprocessing techniques and the characterization of nanomaterials, researchers have not surprisingly discovered many nanomaterials with novel properties, including: nanorods, nanowires, nanobelts, nanosheets and nanofilms. Meanwhile, it has been realized that nanostructures could be assembled into functionalized nanodevices. Certainly, it is important that the essential characteristics of the material are appropriate to the functions of the device. For example, ZnS,[1] ZnSe,[2] $In_2Ge_2O_7$,[3] Ga_2O_3,[4] $K_2Nb_8O_{21}$,[5] Nb_2O_5,[6] and In-doped Ga_2O_3 nanobelts,[7] as well as polystyrene/ZnO core–shell nanofilm,[8] can be used to detect ultraviolet light; CdS,[9] Ta_3N_5,[10] and Sb_2Se_3 nanobelts[11] can be used to detect visible light; CdTe nanobelt-[12] and SnS_2 nanosheet-microsphere film[13] can be used to detect ultraviolet to near-infrared light; and InAs[14] and InAsSb[15] nanowires can be used to detect near-infrared and infrared light. Transition metal dichalcogenides (MX_2) such as MoS_2,[16] WS_2,[17,18] and ZrS_2 (ref. 19) are able to form analogues of graphene because of their layer-like structures,[20] and they show excellent optoelectric properties. Transition metal trichalcogenides (TMTs, MX_3)[21] such as TiS_3,[22] ZrS_3,[23] HfS_3,[24] $TaSe_3$,[25] $NbSe_3$,[25] MoS_3,[26] and so on, are another type of semiconducting or metal compounds. They possess a pseudo one-dimensional (1-D) structure which is a trigonal prism (MX_3) growing along the *b*-axis with a metal atom located at the center and trigonal bases consisting of the chalcogen atoms. Because of the slight change of their chain-like structure, TMTs show anisotropic physical properties, and the corresponding nanomaterials will potentially also show a diversity of properties.[21] However, their nanostructures and devices have not been reported extensively. Nanomaterials and applications of $ZrSe_3$ and $HfSe_3$ are still scarce, or even almost non-existent. In this paper, the preparation and photodetection applications of $ZrSe_3$ and $HfSe_3$ nanobelts is reported.

Results and discussion

Fig. 1a and b display the X-ray diffraction (XRD) patterns of the as-prepared $ZrSe_3$ and $HfSe_3$ nanobelts, respectively. In Fig. 1a, all the diffraction peaks can be properly indexed to $ZrSe_3$ with a monoclinic structure, and are in good agreement with the standard data file (JCPDS no. 36-1338). In Fig. 1b, all the diffraction peaks can also be indexed to $HfSe_3$ with a

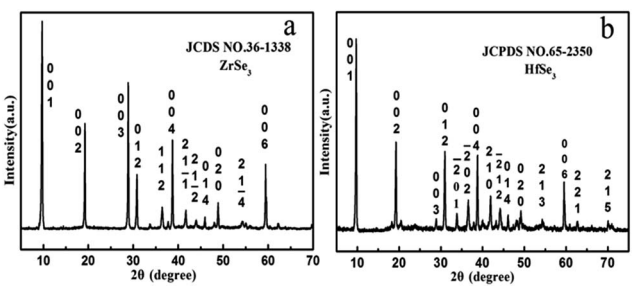

Fig. 1 (a) X-ray diffraction pattern of the $ZrSe_3$ nanobelts. (b) X-ray diffraction pattern of the $HfSe_3$ nanobelts.

School of Chemistry and Chemical Engineering, Key Laboratory of Mesoscopic Chemistry of MOE and State Key Lab of Analytical Chemistry for Life Science, Nanjing University, Nanjing, 210093, P. R. China. E-mail: wuxingca@nju.edu.cn; jjzhu@nju.edu.cn; Fax: +86-25-83317761; Tel: +86-25-83597204

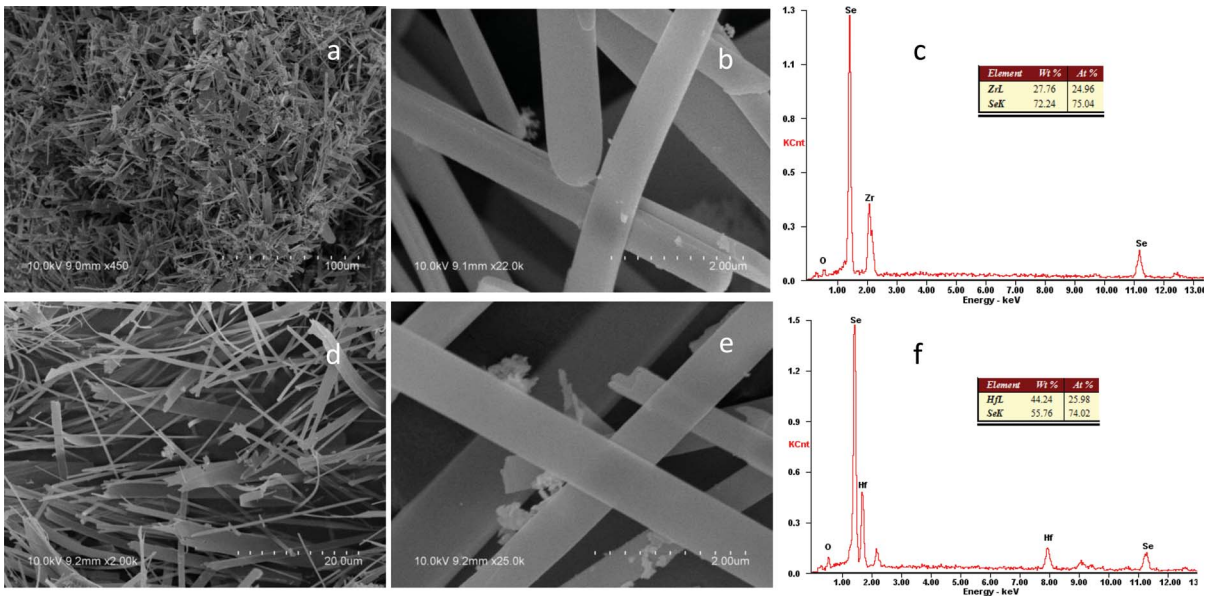

Fig. 2 (a and b) SEM images of the $ZrSe_3$ nanobelts. (c) EDS spectrum of the $ZrSe_3$ nanobelts. (d and e) SEM images of the $HfSe_3$ nanobelts. (f) EDS spectrum of the $HfSe_3$ nanobelts.

monoclinic structure (JCPDS no. 65-2350). No peaks of other impurities were detected, suggesting the formation of pure products. Fig. 2a and b display typical scanning electron microscopy (SEM) images of the as-synthesized $ZrSe_3$ nanobelts, which reveal the formation of a 1-D belt-like nanostructure with a width of 2–500 nm and lengths of up to tens of micrometers, and with a relatively smooth surface. Fig. 2d and e show SEM images of the as-synthesized $HfSe_3$ nanobelts under different magnifications. It is clearly seen that the black products consists of high yield nanobelts, which possess a width of 20–2600 nm and lengths up to tens of micrometers, indicating that they have high aspect ratios. The chemical compositions of the $ZrSe_3$ and $HfSe_3$ nanobelts were measured using energy-dispersive X-ray spectrometry (EDX). The corresponding spectra are shown in Fig. 2c and f, respectively. Atomic ratios of Zr/Se and Hf/Se are close to 1 : 3, indicating that the as-synthesized products are pure, and these results are in good agreement with the XRD results. The detailed structures and orientation of the

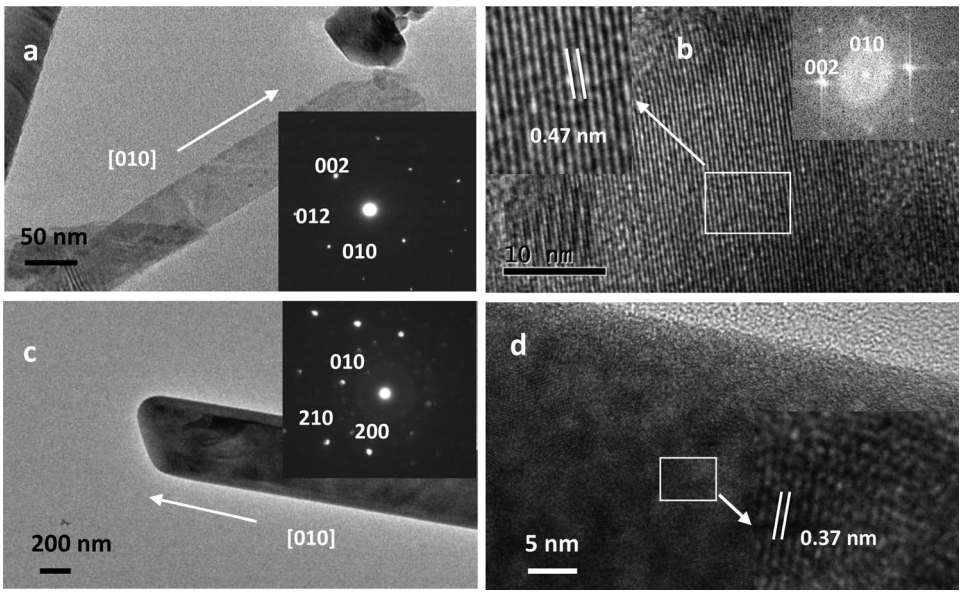

Fig. 3 (a) TEM image and SAED image of a single nanobelt of $ZrSe_3$; the inset is its SAED pattern. (b) HRTEM image of a single nanobelt of $ZrSe_3$; the inset at the upper left corner is a magnification of a part of it, and the inset at the upper right corner is its FFT pattern. (c) TEM image and SAED image of a single nanobelt of $HfSe_3$; the inset is its SAED pattern. (d) HRTEM image of the corresponding $ZrSe_3$ nanobelt; the inset at the lower right corner is a magnification of a part of it.

nanobelts were studied using transmission electron microscopy (TEM), high-resolution TEM (HRTEM), and selected area electron diffraction (SAED).

Fig. 3a shows a TEM image and the SAED pattern (inset in the right-hand lower corner) of an individual $ZrSe_3$ nanobelt. The SAED pattern can be indexed to the monoclinic system of $ZrSe_3$, showing that the nanobelt grew along the [010] direction. Fig 3b is an HRTEM image of the single nanobelt, and its fast Fourier transform (FFT) pattern is displayed at the top left corner. The lattice fringe spacing of 0.47 nm corresponds to the (020) plane of $ZrSe_3$. Fig. 3c shows the TEM image and the SAED pattern (inset in the upper right corner) of an individual $HfSe_3$ nanobelt. The SAED pattern can be indexed to the previously described monoclinic system of $HfSe_3$, showing that the $HfSe_3$ nanobelt grew along the [010] direction. Fig. 3d displays an HRTEM image of the single nanobelt, and the locally magnified part is placed below the right corner, and the lattice fringe space of 0.37 nm corresponds to the (010) plane of $HfSe_3$. So the results reveal that the $ZrSe_3$ and $HfSe_3$ nanobelts are single-crystal.

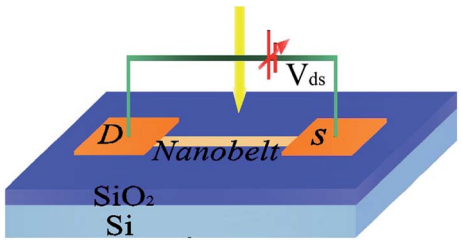

Fig. 4 Schematic illustration of the $ZrSe_3$ and $HfSe_3$ single nanobelt photodetector.

To study the photodetection properties of the as-prepared $ZrSe_3$ and $HfSe_3$ nanobelts, single nanobelt photodetectors were fabricated by deposition of nanobelts on 300 nm silicon dioxide-coated silicon substrate. The patterned titanium (Ti; 10 nm)/gold (Au; 100 nm) electrodes were deposited on the substrate which was sparsely covered by the nanobelts using photolithography, electron-beam deposition and the lift-off process. Fig. 4 shows a schematic illustration of the single nanobelt device and the corresponding SEM images are shown in Fig. 5a and d. The channel width between the two electrodes of the devices is about 5 μm. Fig. 5b and e show the typical current *versus* voltage (*I*–*V*) plots of the single $ZrSe_3$ and $HfSe_3$ nanobelt-based photodetectors in the dark and under illumination with different wavelengths of light, respectively. Nonlinear features of the plots indicate the formation of a Schottky barrier between the Ti/Au electrodes and the nanobelts. Compared with the dark current, the currents of the $ZrSe_3$ device increase obviously under illumination with wavelengths of 405 nm, 650 nm, and 780 nm, indicating that the device shows a good response to visible light. Similarly, the $HfSe_3$ nanobelt photodetector also shows a good response to visible light. Fig. 5c and f display the UV absorption spectra of the $ZrSe_3$ and $HfSe_3$ nanobelts, respectively. It is obvious that both the maximum absorptions are around 640 nm and 530 nm, respectively, which is also consistent with the increased current under illumination with light at different wavelengths.

To study the photosensitive mechanism of the devices, the responses of the photodetectors under different working atmospheres were investigated, as illustrated in Fig. 6. In the air atmospheres, the light illuminated (LI) current of the $ZrSe_3$ photodetector is about 2 times higher than the dark current at a bias of 5 V under 405 nm light illumination of 3.3 mW cm^{-2}, and the LI current of the $HfSe_3$ photodetector is 2.5 times higher

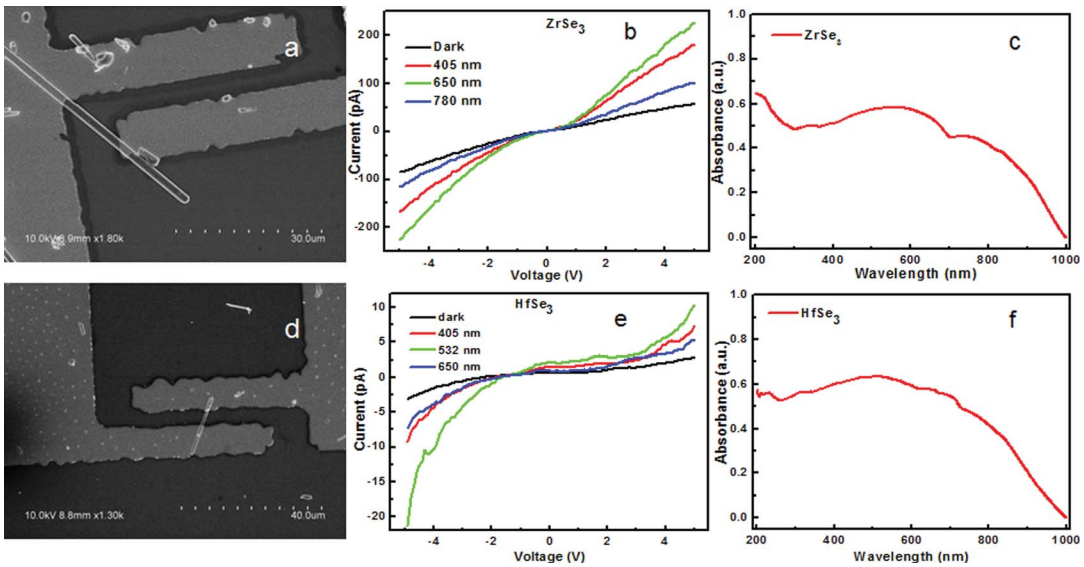

Fig. 5 (a) A typical SEM image of a $ZrSe_3$ single nanobelt photodetector. (b) The *I*–*V* characteristics of the $ZrSe_3$ single nanobelt photodetector under illumination with different wavelengths under light and dark conditions. (c) The ultraviolet-visible (UV-vis) absorption spectrum of $ZrSe_3$ nanobelts. (d) A typical SEM image of an $HfSe_3$ single nanobelt photodetector. (e) The *I*–*V* characteristics of the $HfSe_3$ single nanobelt photodetector under illumination with different wavelengths under light and dark conditions. (f) The UV-vis absorption spectrum of $HfSe_3$ nanobelts.

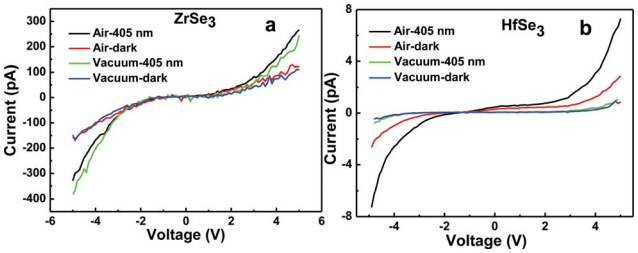

Fig. 6 The *I–V* curves of a single nanobelt photodetector either illuminated with 405 nm light or under dark conditions; and under vacuum or under normal air conditions. (a) $ZeSe_3$ nanobelt photodetector; (b) $HfSe_3$ nanobelt photodetector.

than the dark current under the same conditions. The LI and dark currents of the $ZrSe_3$ photodetector under a vacuum are almost identical to those in air under the same conditions, demonstrating that the currents are not affected by the atmosphere. In contrast, the LI current of the $HfSe_3$ photodetector under a vacuum is about 5 times lower than that in air at a bias of 5 V under 405 nm light illumination of 3.3 mW cm^{-2}. This result is similar to those reported in our previous papers.[24b] In air, oxygen molecules adsorbed onto the surface of the $HfSe_3$ nanobelts captured free electrons from the nanobelts, in agreement with the scheme [$O_2(g) \rightarrow O_2(ad)$; $O_2(ad) + e^- \rightarrow O_2^-$],[27] which creates a high hole conductivity layer near the surface. When the device is illuminated with light, electron hole pairs are generated. The electrons migrate to the surface to be captured by O_2, which results in an increase in hole concentration, so that the photocurrent increases. Under vacuum, oxygen adsorption becomes rare. Therefore, the concentration

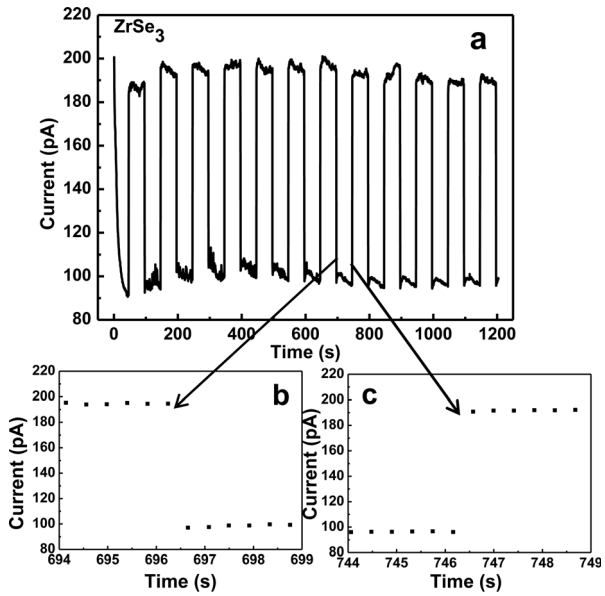

Fig. 7 (a) The reproducible on/off switching of the $ZrSe_3$ single nanobelt photodetector upon 650 nm light illumination. (b) Local amplification decay time figure of the $ZrSe_3$ single nanobelt photodetector. (c) Local amplification rise time figure of the $ZrSe_3$ single nanobelt photodetector.

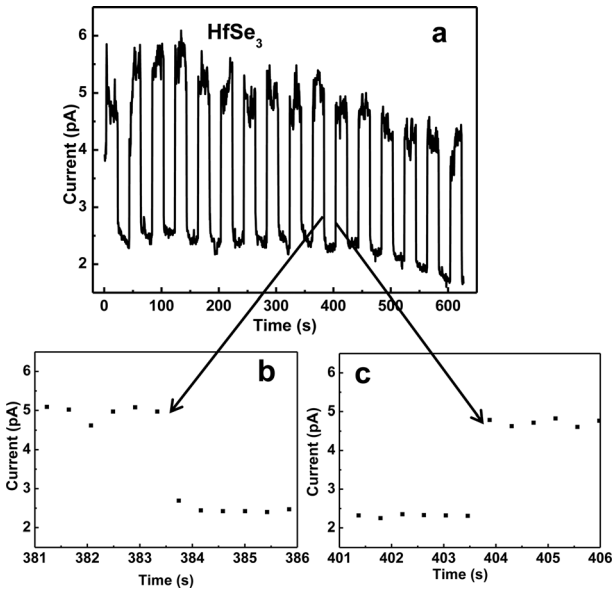

Fig. 8 (a) The reproducible on/off switching of the $HfSe_3$ single nanobelt photodetector with 532 nm light illumination. (b) Local amplification decay time figure of the $HfSe_3$ single nanobelt photodetector (c) local amplification rise time figure of the $HfSe_3$ single nanobelt photodetector.

of holes is lower under vacuum than in air. This explains the cause of the enhancement of photocurrent and dark current in air. In addition, the current is not zero when the applied voltage is zero for the *I–V* characteristics shown in Fig. 5a and 6b. This can be attributed to fact that the instrument has current drift when the applied voltage is very small. The phenomenon has also been reported in other papers.[18] The time responses of $ZrSe_3$ and $HfSe_3$ single nanobelt photodetectors are shown in Fig. 7 and 8, respectively, measured by periodically photoswitching every 50 s at an applied voltage of 5 V (the $ZrSe_3$ photodetector is illuminated by 650 nm light with 3.8 mW cm^{-2}, and the $HfSe_3$ photodetector is illuminated by 532 nm light with 5.3 mW cm^{-2}). The $ZrSe_3$ and $HfSe_3$ single nanobelt photodetectors both show reversible switching between low and high current states with good stability and reproducibility. The LI current of $ZrSe_3$ and $HfSe_3$ single nanobelt photodetectors are about 196.1 pA and 5.1 pA, respectively, and the on/off ratios of currents are 2.1 and 2.2, respectively. The photoresponse time is one of the key factors for detection performance and the relatively faster response time can broaden the scope of the photodetector application. As shown in Fig. 7 and 8, it can be seen that all the rise times and decay times are faster than the limit of our measurement setup (0.4 s), indicating a fast response to the illumination with visible light.

To assess the efficiency of the electron transport and carrier collection, both the responsivity and the quantum efficiency were calculated. The responsivity (R_λ) and quantum efficiency (QE) can be determined from the following equations:[28]

$$R_\lambda = \Delta I/PS$$

$$\mathrm{QE} = hcR_\lambda/e\lambda$$

Table 1 A Comparison of the $ZrSe_3$ and $HfSe_3$ nanobelt photodetectors with other photodetectors

Photodetectors	Wavelength/power	Bias voltage (V)	R_λ (A/W)	QE (%)	Rise time/decay time (s)	Ref.
CdTe nanoribbon	400 nm/637 μW cm^{-2}	5	12	3700	~1.1 s/~3.3 s	12*a*
CdTe nanowire	400 nm/78 μW cm^{-2}	10	80.1	2.5×10^4	0.7 s/1 s	12*b*
Single layer MoS_2	550 nm/80 μW cm^{-2}	1	4.2×10^{-4}		<0.05 s	16*a*
H_2-annealing MoO_3 nanobelt	680 nm/5.6 mW cm^{-2}	0.1	56	1.02×10^4	Void	29
	420 nm/5.6 mW cm^{-2}	0.1	55.5	1.63×10^4		
GaS nanobelt	610 nm/0.5 mW cm^{-2}	2	5.06×10^{-4}	Void	<0.03 s	30
GaS nanobelt	490 nm/0.5 mW cm^{-2}	2	2.3×10^{-4}	Void	<0.03 s	30
$ZrSe_3$ nanobelt	650 nm/3.8 mW cm^{-2}	5	0.53	101	<0.4 s	This work
$HfSe_3$ nanobelt	532 nm/5.3 mW cm^{-2}	5	0.012	2.8	<0.4 s	This work

where ΔI is the difference between the photo-excited current and dark current, P is the light power density irradiated on the individual nanobelt, S is the area of the nanobelt, h is Planck's constant, c is the velocity of the light, e is the electronic charge, and λ is the exciting wavelength. The R_λ and QE of the $ZrSe_3$ and $HfSe_3$ single nanobelt photodetectors are included in Table 1. The R_λ of the $ZrSe_3$ and $HfSe_3$ nanobelt photodetectors are lower than those of the CdTe and hydrogen (H_2)-annealing molybdenum trioxide (MoO_3) nanobelt photodetectors, but are much higher than those of the gallium(II) sulfide (GaS) nanobelt and single layer MoS_2 photodetectors. So $ZrSe_3$ and $HfSe_3$ are still good visible light-sensing materials.

Conclusions

In this work, single crystalline $ZrSe_3$ nanobelts and $HfSe_3$ nanobelts were successfully synthesized using a chemical vapour transport method for the first time. The photodetectors based on a single nanobelt of $ZrSe_3$ or $HfSe_3$ exhibited high sensitivity, stability and a fast response to visible light. These results suggest that $ZrSe_3$ and $HfSe_3$ nanobelts are promising as novels units for nano-optoelectronic devices.

Experimental

Synthesis and characterization

$ZrSe_3$ and $HfSe_3$ nanobelts were directly synthesized using a chemical vapor transport method. In a typical procedure, zirconium (99.95%, 91.2 mg) or hafnium powders (99.9%, 173.8 mg) were first mixed completely with selenium powder (99.99%, 236.9 mg) according to the stoichiometric ratio (1 : 3). Then, the mixtures were sealed in a quartz tube under vacuum (Φ 6 mm × 10 cm, approximately 10^{-2} Pa) and the tube was placed in a conventional horizontal furnace (temperature gradient: approximately 10 K cm^{-1}) with the powders positioned at the center of the furnace. After the furnace had been kept at 650 °C for 24 h, the $HfSe_3$ and $ZrSe_3$ nanobelts had collected on the internal surface of the tubes. The products were characterized using XRD with Cu Kα radiation (Shimadzu XRD-6000), SEM (Hitachi S-4800) with an EDX spectrometer, HRTEM (Jeol JEM-2010) and a UV-vis spectrophotometer (Shimadzu UV-3600).

Device measurements

An appropriate amount of $ZrSe_3$ or $HfSe_3$ nanobelts were suspended in ethanol using ultrasonic mixing for 5 min, and then a drop of this dispersion was dried on an oxidized Si substrate with a 300 nm-thick SiO_2 top layer that serves as a gate oxide. The standard photolithography technique was used to design the source and drain electrodes using Ti/Au (10/100 nm) metal evaporation and a lift-off procedure. The current–voltage (I–V) and the current–time (I–t) characteristic curves of the photodetectors were measured using a Model CRX-4K Cryogenic Probe Station (Lake Shore, Inc.) and a Keithley 2636A source meter (Keithley Instruments Inc.). The photocurrent was illuminated with light of different wavelengths under vacuum and under ambient air conditions. The spectral response for the different wavelengths used was recorded by using different wavelength laser devices. The experiments were done at room temperature in air, except for those which were performed under special conditions.

Acknowledgements

We greatly appreciate the financial support from National Natural Science Foundation of China (NSFC) (no. 21171091 and no. 21335004).

Notes and references

1 (*a*) X. S. Fang, Y. Bando, M. Y. Liao, U. K. Gautam, C. Y. Zhi, B. Dierre, B. D. Liu, T. Y. Zhai, T. Sekiguchi, Y. Koide and D. Golberg, *Adv. Mater.*, 2009, **21**, 2034; (*b*) L. Peng, L. F. Hu and X. S. Fang, *Adv. Mater.*, 2013, **25**, 5321.
2 X. S. Fang, S. L. Xiong, T. Y. Zhai, Y. Bando, M. Y. Liao, U. K. Gautam, Y. Koide, X. G. Zhang, Y. T. Qian and D. Golberg, *Adv. Mater.*, 2009, **21**, 5016.
3 L. Li, P. S. Lee, C. Y. Yan, T. Y. Zhai, X. S. Fang, M. Y. Liao, Y. Koide, Y. Bando and D. Golberg, *Adv. Mater.*, 2010, **22**, 5145.
4 (*a*) L. Li, E. Auer, M. Y. Liao, X. S. Fang, T. Y. Zhai, U. K. Gautam, A. Lugstein, Y. Koide, Y. Bando and D. Golberg, *Nanoscale*, 2011, **3**, 1120; (*b*) W. Feng, X. N. Wang, J. Zhang, L. F. Wang, W. Zheng, P. A. Hu, W. W. Cao and B. Yang, *J. Mater. Chem. C*, 2014, **2**, 3254.

5 H. Liu, Z. M. Zhang, L. F. Hu, N. Gao, L. W. Sang, M. Y. Liao, R. Z. Ma, F. F. Xu and X. S. Fang, *Adv. Opt. Mater.*, 2014, **2**, 771.
6 X. S. Fang, L. F. Hu, K. F. Huo, B. Gao, L. J. Zhao, M. Y. Liao, P. L. Chu, Y. Bando and D. Golberg, *Adv. Funct. Mater.*, 2011, **21**, 3907.
7 W. Tian, C. Y. Zhi, T. Y. Zhai, S. M. Chen, X. Wang, M. Y. Liao, D. Golberg and Y. Bando, *J. Mater. Chem.*, 2012, **22**, 19784.
8 M. Chen, L. F. Hu, J. X. Xu, M. Y. Liao, L. M. Wu and X. S. Fang, *Small*, 2011, **7**, 2449.
9 (*a*) T. Gao, Q. H. Li and T. H. Wang, *Appl. Phys. Lett.*, 2005, **86**, 173105; (*b*) K. M. Deng and L. Li, *Adv. Mater.*, 2014, **26**, 2619.
10 X. C. Wu, Y. R. Tao, L. Li, Y. Bando and D. Golberg, *Nanotechnology*, 2013, **24**, 175701.
11 T. Y. Zhai, M. F. Ye, L. Li, X. S. Fang, M. Y. Liao, Y. F. Li, Y. Koide, Y. Bando and D. Golberg, *Adv. Mater.*, 2010, **22**, 4530.
12 (*a*) X. Xie, S. Y. Kwok, Z. Z. Lu, Y. K. Liu, Y. L. Cao, L. B. Luo, J. A. Zapien, I. Bello, C. S. Lee, S. T. Lee and W. J. Zhang, *Nanoscale*, 2012, **4**, 2914; (*b*) M. Shaygan, K. Davami, N. Kheirabi, C. K. Baek, G. Cuniberti, M. Meyyappan and J. S. Lee, *Phys. Chem. Chem. Phys.*, 2014, **16**, 22687.
13 Y. R. Tao, X. C. Wu, W. Wang and J. N. Wang, *J. Mater. Chem. C*, 2014, DOI: 10.1039/c4tc02325k.
14 Z. Liu, T. Luo, B. Liang, G. Chen, G. Yu, X. M. Xie, D. Chen and G. Z. Shen, *Nano Res.*, 2013, **6**, 775.
15 J. Svensson, N. Anttu, N. Vainorius, B. M. Borg and L.-E. Wernersson, *Nano Lett.*, 2013, **13**, 1380.
16 (*a*) Z. Y. Yin, H. Li, H. Li, L. Jiang, Y. M. Shi, Y. H. Sun, G. Lu, Q. Zhang, X. D. Chen and H. Zhang, *ACS Nano*, 2012, **6**, 74; (*b*) O. Lopez-Sanchz, D. Lembke, M. Kayci, A. Radenovic and A. Kis, *Nat. Nanotechnol.*, 2013, **8**, 497.
17 S. Jo, N. Ubrig, H. Berger, A. B. Kuzmenko and A. F. Morpurgo, *Nano Lett.*, 2014, **14**, 2019.
18 C. Y. Zhang, S. Wang, L. J. Yang, Y. Liu, T. T. Xu, Z. Y. Ning, A. Zak, Z. Y. Zhang, R. Tenne and Q. Chen, *Appl. Phys. Lett.*, 2012, **100**, 243101.
19 (*a*) Y. L. Zhang, X. C. Wu, Y. R. Tao, C. J. Mao and J. J. Zhu, *Chem. Commun.*, 2008, 26832; (*b*) L. Li, X. Fang, T. Y. Zhai, M. Y. Liao, U. K. Gautam, X. C. Wu, Y. Koide, Y. Bando and D. Golberg, *Adv. Mater.*, 2010, **22**, 4151.
20 A. Shmeliov, M. Shannon, P. Wang, J. S. Kim, E. Okunishi, P. D. Nellist, K. Dolui, S. Sanvito and V. Nicolosi, *ACS Nano*, 2014, **8**, 3690.
21 S. K. Srivastava and B. N. Avasthi, *J. Mater. Sci.*, 1992, **27**, 3693.
22 (*a*) J. J. Ma, X. Y. Liu, X. J. Cao, S. H. Feng and M. E. Fleet, *Eur. J. Inorg. Chem.*, 2006, 519; (*b*) X. C. Wu, Y. R. Tao and Q. X. Gao, *Nano Res.*, 2009, **2**, 558.
23 (*a*) L. Y. Huang, K. B. Tang, Q. Yang, G. Z. Shen and S. J. Jia, *Mater. Res. Bull.*, 2004, **39**, 1083; (*b*) Q. X. Gao, X. F. Wang, Y. R. Tao and X. C. Wu, *Sci. Adv. Mater.*, 2012, **4**, 327; (*c*) Y. R. Tao, X. C. Wu and W. W. Xiong, *Small*, 2014, **10**, 4905.
24 (*a*) M. Nath, C. N. R. Rao, R. Popovitz-Biro, A. Albu-Yaron and R. Tenne, *Chem. Mater.*, 2004, **16**, 2238; (*b*) W. W. Xiong, J. Q. Chen, X. C. Wu and J. J. Zhu, *J. Mater. Chem. C*, 2014, **2**, 7392.
25 (*a*) A. V. Zavalko and S. V. Zaitsev-Zotov, *J. Phys. IV*, 2005, **131**, 359; (*b*) X. C. Wu, Y. R. Tao, L. Li, T. Y. Zhai, Y. Bando and D. Golberg, *J. Nanosci. Nanotechnol.*, 2011, **11**, 10123.
26 M. L. Tang, D. C. Grauer, B. Lassalle-Kaiser, V. K. Yachandra, L. Amirav, J. R. Long, J. Yano and A. P. Alivisatos, *Angew. Chem., Int. Ed.*, 2011, **123**, 10385.
27 C. L. Hus, H. H. Li and T. J. Hsueh, *ACS Appl. Mater. Interfaces*, 2013, **5**, 11142.
28 L. F. Hu, J. Yan, M. Y. Liao, H. J. Xiang, X. G. Gong, L. D. Zhang and X. S. Fang, *Adv. Mater.*, 2012, **24**, 2305.
29 D. Xiang, C. Han, J. L. Zhang and W. Chen, *Sci. Rep.*, 2014, **4**, 4891.
30 P. A. Hu, L. F. Wang, M. Yoon, J. Zhang, W. Feng, X. N. Wang, Z. Z. Wen, J. C. Idrobo, Y. Miyamoto, D. B. Geohegan and K. Xiao, *Nano Lett.*, 2013, **13**, 1649.

